

Superhigh thermoelectric figure of merit in silver halides AgCl and AgBr from first principles

Xiuxian Yang,¹ Zhenhong Dai,^{1,*} Yinchang Zhao,^{1,†} and Sheng Meng^{2,3,‡}

¹*School of Opto-electronic Information Science and Technology,
Yantai University, Yantai 264005, People's Republic of China*

²*Beijing National Laboratory for Condensed Matter Physics and Institute of Physics,
Chinese Academy of Sciences, Beijing,
100190, People's Republic of China*

³*Collaborative Innovation Center of Quantum Matter,
Beijing 100084, People's Republic of China*

(Dated: April 15, 2019)

Abstract

Searching for the high-performance thermoelectric (TE) materials has always been a long-held dream in the thermoelectricity field. Recently, it is found in experiments that the largest figure of merit ZT of 2.6 can be reached in SnSe crystals at 923 K and Cu₂Se sample at 850 K, which arouses the enormous interest of seeking high- ZT materials. Based on first-principle calculations and Boltzman transport equation (BTE), we report in this letter that silver halides (AgCl and AgBr) in rocksalt structure have excellent TE performances. A superhigh ZT of about 7.0 at mid-temperature (~ 600 K) is obtained in the p -type doped AgCl and AgBr crystals, which far exceeds the ZT values of all current bulk TE materials. This record-breaking ZT value is attributed to the ultralow intrinsic lattice thermal conductivity κ_L (e.g. $\kappa_L \sim 0.10$ and 0.09 Wm⁻¹K⁻¹ for AgCl and AgBr at 600 K, respectively). Our results may be a feat that could revolutionize the field of the heat energy conversion.

PACS numbers: 65.40.-b, 66.70.-f, 63.20.-e, 72.20.-i

* zhdai@ytu.edu.cn

† y.zhao@ytu.edu.cn

‡ smeng@iphy.ac.cn

I. INTRODUCTION

The thermoelectric (TE) technology provides a simple and environmentally friendly solution for direct conversion from heat to electricity, which has drawn a good deal of attentions[1–7]. However, due to lacking significant progress in lead-free, efficient TE devices, the influence of TE technology has mainly remained within a small sphere of niche applications[8, 9]. The efficiency of a TE material is determined by the figure of merit ZT defined as

$$ZT = \frac{S^2\sigma T}{\kappa_e + \kappa_L}, \quad (1)$$

where S is the Seebeck coefficient, σ is the electrical conductivity, T is the temperature in kelvin, κ_e represents thermal conductivity of the charge carrier and κ_L is that of the lattice. Currently, the ZT values of most typical bulk TE materials, such as PbTe, n -Type skutterudites CoSb₃, PbSe, Bi₂Te₃, nanocomposites and p -type half-Heusler are in the range of 1.5 \sim 2.5[10–16]. Due to the interdependent relationship in σ , S and κ , it is usually difficult to improve an average ZT well above 2.5. In the past decade, there are several approaches proposed to improve ZT , including the enhancement of electronic properties (S and σ) (by doping electron or hole[17, 18], introducing the resonant states in the vicinity of Fermi level[19–21], and band convergence[22, 23]) and the reduction of the κ_L (by enhancing phonon scattering through disorder within the unit cell[24, 25] or forming solid solutions[22, 26]).

So far, the largest ZT value of 2.6 in experiment can be reached in SnSe crystals at 923 K and Cu₂Se sample at 850 K[8, 9]. In SnSe crystals the excellent TE performance stems from the ultralow thermal conductivity, such as $\kappa_L \sim 0.23 \pm 0.03 \text{ Wm}^{-1}\text{K}^{-1}$ at 973 K, while the remarkable TE performance in Cu₂Se sample is attributed to the localization of Cu⁺ induced by the incorporation of indium (In) into the Cu₂Se lattice, which enhances the σ and reduces the κ_L of the nanocomposites simultaneously[8, 9]. A common feature in these materials is the presence of low κ_L , which is a crucial ingredient of high- ZT materials. Therefore, searching for TE materials with low intrinsic κ_L is our striving directions. In 1986, M. V. Smirnov *et al.* reported that molten alkali halides and their mixtures have ultralow κ_L , e.g., the $\kappa_L \sim 0.2 - 1.4 \text{ W/mK}$ in the temperature range of 900 \sim 1300 K[27], which inspires us to study the heat transport and TE properties of halide materials. In this work, we present that the silver halides AgCl and AgBr crystals materials may be the best candidates for

high TE performance.

For AgCl and AgBr, the theoretical and experimental studies are only focused on the electronic structure properties, ionic transport properties, optical absorption and response or other chemical properties in the past few decades[28–33]. In the practical applications, AgCl is a common reference electrode in electrochemistry, while AgBr is widely used in photographic films. Nevertheless, to date the study of the heat transport properties and TE properties in these materials is lacking, which is may be due to the low melting point (728 K for AgCl, 701 K for AgBr)[28, 29]. In this paper, we systematically investigate the heat and electronic transport properties of AgCl and AgBr, and conclude that they have ultralow intrinsic κ_L , high S, and consequently remarkable TE performances.

II. METHODOLOGY

Using first-principle calculations and Boltzman transport equation (BTE), we study the electronic structure, lattice thermal transport and electron transport properties of AgCl and AgBr crystals with rocksalt structure. The calculations are performed by the Vienna Ab-initio Simulation Package (VASP)[34, 35], which is based on the density functional theory (DFT). In the DFT calculations, a 520 eV energy cutoff with the exchange-correlation functional of generalized gradient approximation (GGA) of the Perdew-Burke-Ernzerhof (PBE)[36] is used to simulate the valence electron. A $25 \times 25 \times 25$ k-point is utilized for the electron-momentum integration. We use the ShengBTE[37] package to calculate the lattice thermal conductivity with a $30 \times 30 \times 30$ q-mesh. The only input parameters are the harmonic and anharmonic interatomic force constants (IFCs). The harmonic IFCs were obtained based on the finite-difference approach via the PHONOPY program[38] within the $5 \times 5 \times 5$ supercells, and the anharmonic IFCs were created by thirdorder.py script[37] within the $5 \times 5 \times 5$ supercells. In the anharmonic IFCs calculations, the eight nearest neighbor interactions were taken into account.

To obtain the electron transport properties, we use the rigid-band approach and the semiclassical Boltzmann theory, which is performed in the BOLTZTRAP code[39]. In this approach, the constant scattering time approximation τ is used, which is the only parameter that can be tuned. The value of τ from 1 to 8 fs is used to obtain relatively reasonable results. The electronic structure is recalculated by VASP on the dense k-points of $80 \times 80 \times 80$ to

TABLE I. The lattice constant a (\AA), volume V ($\text{\AA}^3/(\text{unit cell})$), comparison of band-gap (eV) obtained in GGA and GW theoretical calculations compared with experimental values, the melting point of AgCl and AgBr crystals.

Crystal	a \AA	V $\text{\AA}^3/\text{unit cell}$	E_{gap}^{GGA} eV	E_{gap}^{GW} eV	$E_{gap}(\text{Ex})$ eV	melting point K
AgCl	5.60	44.02	0.95	3.28	3.0(Ref.[40])	728(Ref.[28, 29])
AgBr	5.85	49.82	0.70	2.70	2.5(Ref.[40])	701(Ref.[28, 29])

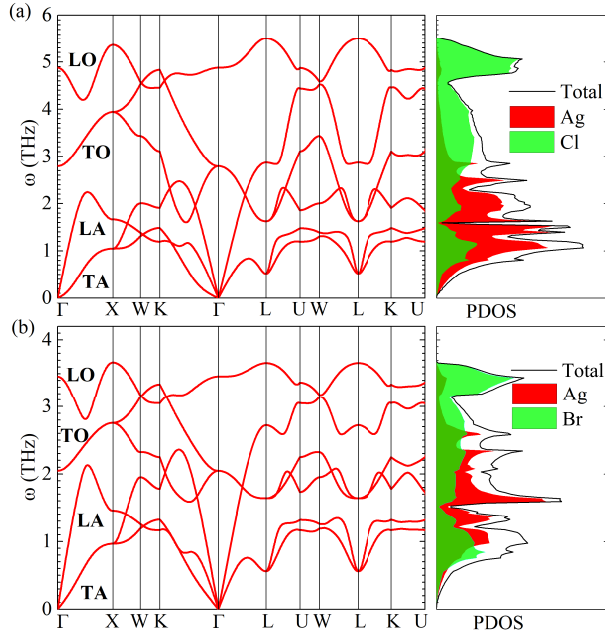


FIG. 1. (Color online). Calculating phonon dispersion relations and phonon density of states (PDOS) of AgCl (a) and AgBr (b) along the high symmetry point within the first Brillouin zone (BZ), respectively.

acquire precise derivatives of the Kohn-Sham eigenvalues.

III. RESULTS AND DISCUSSION

AgCl and AgBr crystals are stable in the rocksalt structures (as shown in Supplemental S. 1) below their melting point (728 K for AgCl, 701 K for AgBr)[28, 29]. Their optimized lattice constants a are 5.60 Å and 5.85 Å, respectively, as shown in TABLE I, which are slightly larger than the experimental values of 5.55 Å for AgCl and 5.774 Å for AgBr[30], this is due to the fact that GGA often overestimates the lattice constant. Usually, the phonon spectrum can inspect the structure stability, which lies in the fact that for each phonon mode the frequency should be a real quantity and not imaginary[41]. Figure 1 illustrates the phonon dispersion spectrum and phonon density of states (PDOS) of AgCl and AgBr. Obviously, there are no imaginary frequencies in the phonon spectrum, indicating that these crystals are stable structures. In our calculations, phonon spectrum of AgCl and AgBr are consistent with other theoretical calculation and experimental data[42–44], which indicates the accuracy of our calculations. There are six phonon modes: two transverse acoustic modes (TA), one longitudinal acoustic mode (LA), two transverse optic modes (TO) and one longitudinal optic mode (LO) in the phonon spectrum due to the existence of two atoms in the unit cell. The optic modes exhibit large splitting of TO and LO modes around the Γ point because of the strong coupling between the lattice and polarization field. The polarization field is induced by the longitudinal optic modes in the phonon long-wavelength limit in the ionic crystals. The polarization field depends on the dielectric constants and the Born effective charges computed by the density functional perturbation theory (DFPT) in the VASP code. For AgCl (AgBr), the Born effective charges of Ag atom and halogen atom are 1.45 (1.53) e and -1.45 (-1.53) e , respectively, and the dielectric constant is 4.94 (5.87), indicating a strong polarization field and thus resulting in a large TO/LO splitting of about 2.13 (1.42) THz, as presented in Fig. 1. The partial PDOS shows that for AgCl the acoustic modes are mainly afforded by the Ag atom, while for AgBr the acoustic modes are afforded by the combination of Ag atom and Br atom. This is attributed to the difference of the atomic effective mass.

Figure 2 gives intrinsic κ_L of AgCl and AgBr versus temperature from 100 to 700 K. These silver halide materials have smaller discrepancy of κ_L and exhibit similar $\kappa_L \propto T^{-1}$ trend. Since more phonons are active under high temperature, the Umklapp process will become critical in the phonon scattering and reduce the κ_L [45]. Remarkable, the values

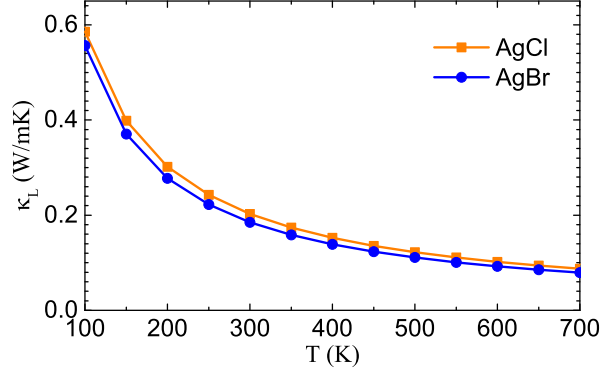


FIG. 2. (Color online). The lattice thermal conductivity κ_L versus temperature T for AgCl and AgBr. The orange square and blue circle lines represent the κ_L for AgCl and AgBr, respectively.

of κ_L are fairly low. For instance, the κ_L of 0.202 (0.102) and 0.185 (0.093) $\text{Wm}^{-1}\text{K}^{-1}$ are obtained at 300 (600) K in AgCl and AgBr crystals, respectively. These values of κ_L are much lower than the commercial TE materials PbTe ($1.40 - 2.85 \text{ Wm}^{-1}\text{K}^{-1}$ at 300 K) and its alloys (1.78 and $1.42 \text{ Wm}^{-1}\text{K}^{-1}$ for $\text{Pb}_{0.94}\text{Mg}_{0.06}\text{Te}$ and $\text{Pb}_{0.8}\text{Mg}_{0.2}\text{Te}$ at 300 K, respectively.)[10]. Furthermore, to gain insight into the heat transport mechanism and decide which phonon modes provide the primary heat conductivity, the accumulative lattice thermal conductivity κ_a scaled by the total κ_L as a function of frequency, which exhibits the summed contributions from the phonon modes below the specified frequency, is also calculated, as shown in Supplemental S.2. For AgCl (AgBr), more than 80% of the heat transport is induced by the phonons with the frequency below 3 (2) THz. Based on the combination of S.2 and Fig. 1, we can find that three acoustic phonon modes and two TO modes dominate the heat transport. In addition, the ultralow κ_L usually hints excellent TE performance if their power factor $S^2\sigma$ (PF) and electronic transport properties are good enough.

The electronic structure diagrams of AgCl and AgBr are shown in Supplemental S. 3(a-b), which are obtained from GGA method. The GGA results show that AgCl and AgBr are indirect band gap semiconductors with the band gap values of 0.95 and 0.70 eV. The conduction band minima (CBM) locates at the high-symmetry L point and valence band maxima (VBM) locates at the high-symmetry Γ point. It must be point out that the GGA results are much lower than the experimental values (such as, 3.0 eV for AgCl and 2.5 eV for AgBr[40]), as shown in TABLE I. Therefore, we used the GW_0 method[46–49] to recalculate

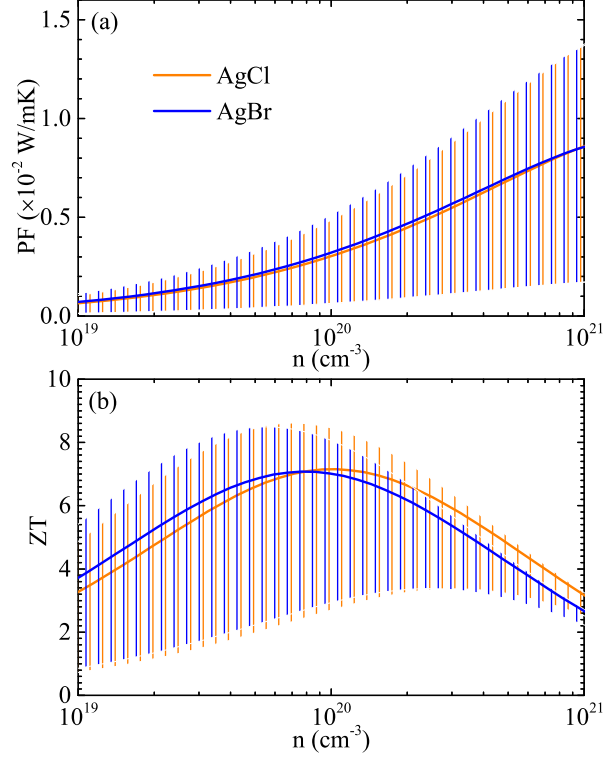


FIG. 3. (Color online). At 600 K, the TE parameters: (a) the power factor (PF) $S^2\sigma$ and (b) figure of merit ZT for the p-type doped AgCl (orange curves) and AgBr (blue curves) as a function of carrier concentration. In these panels, the lower and upper limits of the vertical bars and the full curves represent the values with $\tau = 1, 8$ and 5 fs, respectively.

the electronic band structure. These results are shown in Supplemental S. 3(c-d) and TABLE I. The GW_0 results reveal that AgCl and AgBr are also indirect band gap semiconductors but with the wide band gap of 3.28 and 2.70 eV, which are consistent with the experimental values. Since the electronic transport properties are determined by the electronic energy band structure, the project band structure diagrams and partial electronic density of states (EDOS) for AgCl and AgBr calculated with GGA are shown in Supplemental S. 4(a-b), respectively. The partial EDOS shows that the valence band close to Fermi level is mainly contributed by the Ag atom d orbital and halogen atom p orbital. The dispersion of energy band structure reveals both heavy and light effective masses of charge carriers. The flat band is in the valence band along Γ -K line, making a large EDOS and heavy effective masses, which leads to high thermal power S. In contrast, the strong dispersion are observed in both valence band along K- Γ -L line and conduction band minimum, which indicates a high

electron mobility, μ . Thus, according to the equation of $\sigma = nq\mu$, here n is the carrier concentration, q is quantity of electric charge and σ is the electrical conductivity. Thus, a high σ can be expected, if n is high enough.

To evaluate the electronic transport and TE properties, the S , σ/τ and κ_e were calculated by the BOLTZTRAP code[39] as a function of temperature and carrier concentration n . The calculations with the scissors shift of 2.33 and 2.0 eV ($E_{gap}^{GW_0} - E_{gap}^{GGA}$) for AgCl and AgBr crystals, are also performed. The results show that band gap underestimate have no effect on electronic transport properties. Additionally, the best TE performances are obtained in p -type doped AgCl and AgBr crystals, while n -type doping cases show bad TE performance, as shown in Supplemental S. 5, thus we no longer care about the n -type doping cases for these materials in the following discussion.

The calculated thermal power S is shown in Supplemental S. 6. The S increases with temperature at the same carrier concentration and decreases with carrier concentration at the same temperature, similar to the tendency in most of semiconducting TE materials[3]. The S values are much high. For instance, the values of S for AgCl (AgBr) are in the range of $350 \sim 430$ ($330 \sim 410$) $\mu V/K$ at $n \sim 10^{20} \text{ cm}^{-3}$ as the temperature increases from 300 to 600 K. These values of S are much larger than PbTe, such as the values of S are in the range of $100 \sim 300 \mu V/K$ at $300 \sim 600$ K[50]. In addition, the values of S of AgCl are higher than that of AgBr at the same temperature, indicating that a possible higher ZT in AgCl. Although the σ and κ_e values are not confirmed at present, the combination of large S and ultralow κ_L suggest a possible high ZT in AgCl and AgBr. To calculate σ and κ_e , we should estimate the amplitude of electronic scattering times τ and consider the effect of lattice vibration on practical τ , thus we use τ from 1 to 8 fs to obtain a reasonable result, as shown in Supplemental S. 7 and S. 8. We find that the σ values does not rely on temperature, which is in accordance with the electronic Boltzmann theory[39]. The values of σ of AgCl are slightly smaller than that of AgBr. Moreover, to obtain the accuracy ZT values, it is necessary to calculate the κ_e , although the values of κ_e are much lower than the κ_L . These results are presented in Supplemental S. 8 at 300, 500 and 600 K for AgCl and AgBr, respectively. One can find that the values of κ_e of AgBr are slightly higher than that of AgCl in the temperature range $300 \sim 600$ K.

Next, the power factor (PF) and ZT for p -type doped AgCl and AgBr as a function of carrier concentration at 600 K are shown in Fig. 3(a) and (b). In these panels, the lower

and upper limits of the vertical bars and the full curves represent the values with $\tau = 1, 8$ and 5 fs, respectively. The PF curves of AgBr are slightly higher than that of AgCl mainly due to the higher σ in AgBr crystal. The values of ZT with $\tau = 1 \sim 8$ fs in the wide carrier concentration region ($n = 10^{17} \sim 10^{22} \text{ cm}^{-3}$) at 300, 500 and 600 K for AgCl and AgBr are presented in Supplemental S. 9(a-c). For AgCl, with $\tau = 8$ fs, the extraordinarily high ZT of 8.62 is obtained at 600 K and $n \approx 7.32 \times 10^{19} \text{ cm}^{-3}$ when $\text{PF} \sim 0.41 \text{ Wm}^{-1}\text{K}^{-1}$. As τ decreases to 5 fs, a fairly large ZT is 7.23 in higher n ($\sim 1 \times 10^{20} \text{ cm}^{-3}$) when $\text{PF} \sim 0.32 \text{ Wm}^{-1}\text{K}^{-1}$. Even with $\tau = 1$ fs, a large ZT (3.44) is also achieved in $n \sim 3.24 \times 10^{20} \text{ cm}^{-3}$ when $\text{PF} \sim 0.11 \text{ Wm}^{-1}\text{K}^{-1}$. For AgBr, with $\tau = 8$ fs, the extraordinarily high ZT of 8.46 is obtained at 600 K and $n \approx 5.36 \times 10^{19} \text{ cm}^{-3}$ when $\text{PF} \sim 0.35 \text{ Wm}^{-1}\text{K}^{-1}$. A fairly large ZT of 7.01 is obtained in $n \approx 8.12 \times 10^{19} \text{ cm}^{-3}$ as τ decreases to 5 fs when PF is $0.29 \text{ Wm}^{-1}\text{K}^{-1}$. As τ further decreases to 1 fs, ZT of 3.49 is also larger with higher n ($\sim 2.49 \times 10^{20} \text{ cm}^{-3}$) when PF is $0.11 \text{ Wm}^{-1}\text{K}^{-1}$. It should be noted that the maximum ZT need lower carrier concentration as τ increases. At the lower temperature, such as 300 K, AgCl and AgBr also exhibit excellent TE performance. The high ZT values are 3.09 and 2.39 for AgCl when τ is 8 and 5 fs, respectively, as shown in Supplemental S. 9(a) the real curves. For AgBr, the ZT values are 2.89 and 2.25 when τ is 8 and 5 fs, respectively, as shown in Supplemental S. 9(a) the dash curves. At 500 K, for AgCl (AgBr) the ZT values are 6.83 (6.72) and 5.60 (5.49) when τ is 8 and 5 fs, respectively, as shown in Supplemental S. 9(b). One can find that large PF can lead to a high ZT, meanwhile being subject to κ_e and κ_L , which indicates a compromise between the PF and κ and a complex competition mechanism within the TE materials. Our results suggest that AgCl and AgBr crystals in rocksalt structure have unprecedented large ZT values, which are highest than that of all current bulk TE materials. Finally, we must point out that due to the property of unusual sensitivity to light for these materials, a black shell is needed to design TE devices, meanwhile ensuring that the operating temperature of devices is lower than their melting point.

IV. CONCLUSION

To summarize, we have calculated electronic structure, lattice thermal transport and electronic transport properties of rocksalt structure AgCl and AgBr crystals, which is employed first principles and phonon (electron) Boltzmann transport theory. The ultralow κ_L

of 0.202 and 0.185 $\text{Wm}^{-1}\text{K}^{-1}$ of AgCl and AgBr are obtained at the room temperature. Usually, the ultralow κ_L indicates the excellent TE performances, hence a combination of the first principle calculations and the semiclassical analysis was used to investigate the TE properties for these materials. The electronic transport properties are determined by the electronic energy band structure. We find that the flat band leads to high S and highly dispersive band results in good σ . Therefore, the unprecedentedly large values of ZT of 7.2 and 7.1 are obtained at 600 K in the p-type doped AgCl and AgBr, which is defeated the ZT values of all current bulk TE materials. These results indicate that AgCl and AgBr are excellent mid-temperature (500 – 900 K) power generation materials, although we need a black shell and the operating temperature of devices is below their melting point.

V. ACKNOWLEDGMENT

This research were supported by the National Natural Science Foundation of China under Grant No.11774396 and No.11704322, Shandong Natural Science Funds for Doctoral Program under Grant No.ZR2017BA017, the National Key Research and Development Program of China under Grant No.2016YFA0300902, and Graduate Innovation Foundation of Yantai University, GIFYTU, No.YDZD1810.

-
- [1] J. He and T. M. Tritt, *Science* **357** (2017), 10.1126/science.aak9997.
 - [2] G. J. Snyder and E. S. Toberer, *Nature Materials* **7**, 105 (2008).
 - [3] Y. Zhao, Z. Dai, C. Zhang, C. Lian, S. Zeng, G. Li, S. Meng, and J. Ni, *Phys. Rev. B* **95**, 014307 (2017).
 - [4] X. Su, P. Wei, H. Li, W. Liu, Y. Yan, P. Li, C. Su, C. Xie, W. Zhao, P. Zhai, Q. Zhang, X. Tang, and C. Uher, *Advanced Materials* **29**, 1602013 (2017), 1602013.
 - [5] L. E. Bell, *Science* **321**, 1457 (2008).
 - [6] J. He, S. N. Girard, M. G. Kanatzidis, and V. P. Dravid, *Advanced Functional Materials* **20**, 764 (2010).
 - [7] J. P. Heremans, C. M. Thrush, D. T. Morelli, and M.-C. Wu, *Phys. Rev. Lett.* **88**, 216801 (2002).

- [8] L.-D. Zhao, S.-H. Lo, Y. Zhang, H. Sun, G. Tan, C. Uher, C. Wolverton, V. P. Dravid, and M. G. Kanatzidis, *Nature* **508** (2014), 10.1038/nature13184.
- [9] A. A. Olvera, N. A. Moroz, P. Sahoo, P. Ren, T. P. Bailey, A. A. Page, C. Uher, and P. F. P. Poudeu, *Energy Environ. Sci.* **10**, 1668 (2017).
- [10] T. Fu, X. Yue, H. Wu, C. Fu, T. Zhu, X. Liu, L. Hu, P. Ying, J. He, and X. Zhao, *Journal of Materiomics* **2**, 141 (2016), special Issue on Advances in Thermoelectric Research.
- [11] G. Rogl, A. Grytsiv, P. Rogl, N. Peranio, E. Bauer, M. Zehetbauer, and O. Eibl, *Acta Materialia* **63**, 30 (2014).
- [12] H. Wang, Y. Pei, A. D. LaLonde, and G. J. Snyder, *Proceedings of the National Academy of Sciences* **109**, 9705 (2012).
- [13] M. Ibez, Z. Luo, A. Gen, L. Piveteau, S. Ortega, D. Cadavid, O. Dobrozhan, Y. Liu, M. Nachttegaal, M. Zebarjadi, J. Arbiol, M. V. Kovalenko, and A. Cabot, *Nature Communications* **7** (2016), 10.1038/ncomms10766.
- [14] A. T. Duong, V. Q. Nguyen, G. Duvjir, V. T. Duong, S. Kwon, J. Y. Song, J. K. Lee, J. E. Lee, S. Park, T. Min, J. Lee, J. Kim, and S. Cho, *Nature Communications* **7** (2016), 10.1038/ncomms13713.
- [15] C. Fu, S. Bai, Y. Liu, Y. Tang, L. Chen, X. Zhao, and T. Zhu, *Nature Communications* **6** (2015), 10.1038/ncomms9144.
- [16] S. I. Kim, K. H. Lee, H. A. Mun, H. S. Kim, S. W. Hwang, J. W. Roh, D. J. Yang, W. H. Shin, X. S. Li, Y. H. Lee, G. J. Snyder, and S. W. Kim, *Science* **348**, 109 (2015).
- [17] M. Zebarjadi, G. Joshi, G. Zhu, B. Yu, A. Minnich, Y. Lan, X. Wang, M. Dresselhaus, Z. Ren, and G. Chen, *Nano letters* **11**, 2225 (2011).
- [18] B. Yu, M. Zebarjadi, H. Wang, K. Lukas, H. Wang, D. Wang, C. Opeil, M. Dresselhaus, G. Chen, and Z. Ren, *Nano letters* **12**, 2077 (2012).
- [19] J. P. Heremans, B. Wiendlocha, and A. M. Chamoire, *Energy & Environmental Science* **5**, 5510 (2012).
- [20] J. P. Heremans, V. Jovovic, E. S. Toberer, A. Saramat, K. Kurosaki, A. Charoenphakdee, S. Yamanaka, and G. J. Snyder, *Science* **321**, 554 (2008).
- [21] A. Minnich, M. Dresselhaus, Z. Ren, and G. Chen, *Energy & Environmental Science* **2**, 466 (2009).

- [22] W. Liu, X. Tan, K. Yin, H. Liu, X. Tang, J. Shi, Q. Zhang, and C. Uher, *Physical review letters* **108**, 166601 (2012).
- [23] X. Liu, T. Zhu, H. Wang, L. Hu, H. Xie, G. Jiang, G. J. Snyder, and X. Zhao, *Advanced Energy Materials* **3**, 1238 (2013).
- [24] T. Markussen, A.-P. Jauho, and M. Brandbyge, *Physical Review B* **79**, 035415 (2009).
- [25] S. Bhattacharya, R. Hermann, V. Keppens, T. Tritt, and G. Snyder, *Physical Review B* **74**, 134108 (2006).
- [26] P. F. Poudeu, J. D'Angelo, H. Kong, A. Downey, J. L. Short, R. Pcionek, T. P. Hogan, C. Uher, and M. G. Kanatzidis, *Journal of the American Chemical Society* **128**, 14347 (2006).
- [27] M. Smirnov, V. Khokhlov, and E. Filatov, *Electrochimica acta* **32**, 1019 (1987).
- [28] . Tasseven, J. Trulls, O. Alcaraz, M. Silbert, and A. Gir, *The Journal of Chemical Physics* **106**, 7286 (1997).
- [29] J. K. Aboagye and R. J. Friauf, *Phys. Rev. B* **11**, 1654 (1975).
- [30] C. R. Berry, *Phys. Rev.* **97**, 676 (1955).
- [31] B. L. Joesten and F. C. Brown, *Physical Review* **148**, 919 (1966).
- [32] N. J. Carrera and F. C. Brown, *Physical Review B* **4**, 3651 (1971).
- [33] F. Bassani, R. S. Knox, and W. B. Fowler, *Phys. Rev.* **137**, A1217 (1965).
- [34] G. Kresse and J. Furthmller, *Computational Materials Science* **6**, 15 (1996).
- [35] A. Togo, F. Oba, and I. Tanaka, *Phys. Rev. B* **78**, 134106 (2008).
- [36] J. P. Perdew, K. Burke, and M. Ernzerhof, *Phys. Rev. Lett.* **77**, 3865 (1996).
- [37] W. Li, J. Carrete, N. A. Katcho, and N. Mingo, *Computer Physics Communications* **185**, 1747 (2014).
- [38] A. Togo, F. Oba, and I. Tanaka, *Physical Review B* **78**, 134106 (2008).
- [39] G. K. Madsen and D. J. Singh, *Computer Physics Communications* **175**, 67 (2006).
- [40] R. H. Victora, *Phys. Rev. B* **56**, 4417 (1997).
- [41] A. Togo and I. Tanaka, *Scripta Materialia* **108**, 1 (2015).
- [42] Y. Li, L. Zhang, T. Cui, Y. Ma, G. Zou, and D. D. Klug, *Phys. Rev. B* **74**, 054102 (2006).
- [43] S. Vaidya and G. Kennedy, *Journal of Physics and Chemistry of Solids* **32**, 951 (1971).
- [44] B. Dorner, *J. Phys. c* **9**, 723 (1976).
- [45] Y. Ding and Y. Wang, *Applied Surface Science* **396**, 1164 (2017).
- [46] M. Shishkin and G. Kresse, *Phys. Rev. B* **75**, 235102 (2007).

- [47] F. Fuchs, J. Furthmüller, F. Bechstedt, M. Shishkin, and G. Kresse, Phys. Rev. B **76**, 115109 (2007).
- [48] M. Shishkin and G. Kresse, Phys. Rev. B **74**, 035101 (2006).
- [49] M. Shishkin, M. Marsman, and G. Kresse, Phys. Rev. Lett. **99**, 246403 (2007).
- [50] J. P. Heremans, V. Jovovic, E. S. Toberer, A. Saramat, K. Kurosaki, A. Charoenphakdee, S. Yamanaka, and G. J. Snyder, Science **321**, 554 (2008).